Colloids and Surfaces A: Physicochemical and Engineering Aspects 647 (2022) 129095

Contents lists available at ScienceDirect

Colloids and Surfaces A: Physicochemical and Engineering Aspects

journal homepage: www.elsevier.com/locate/colsurfa

Impact of fluorescent dyes on the physicochemical parameters of microbubbles stabilized by albumin-dye complex

Roman A. Barmin [a,*], Polina G. Rudakovskaya [a], Vasiliy S. Chernyshev [a], Olga I. Guslyakova [b], Olga A. Sindeeva [a], Ekaterina S. Prikhozhdenko [b], Daniil N. Bratashov [b], Arkady S. Abdurashitov [a], Elizaveta A. Maksimova [a], Polina A. Demina [c,d], Evgeny V. Khaydukov [c,e], Alexey V. Gayer [f], Evgeny A. Shirshin [e,f,g], Alexander A. Solovev [h], Yongfeng Mei [h], Dmitry A. Gorin [a,*]

[a] Skolkovo Institute of Science and Technology, 3 Nobelya Str., Moscow 121205, Russia
[b] Saratov State University, 83 Astrakhanskaya Str., Saratov 410012, Russia
[c] FSRC "Crystallography and Photonics" RAS, Leninskiy Prospekt 59, 119333, Moscow, Russia
[d] Shemyakin-Ovchinnikov Institute of Bioorganic Chemistry RAS, Miklukho-Maklaya str. 16/10, 117997 Moscow, Russia
[e] I.M. Sechenov First Moscow State Medical University, Trubetskaya str. 8-2, Moscow 119991, Russia
[f] Lomonosov Moscow State University, 1/2 Leninskie Gory, Moscow 119991, Russia
[g] Institute of Spectroscopy of the Russian Academy of Sciences, 5 Fizicheskaya Str., Troitsk, Moscow 108840, Russia
[h] Fudan University, 220 Handan Road, Shanghai 200433, People's Republic of China

HIGHLIGHTS

- Dye hydrophobicity impacted the surface tension of solutions used for microbubble preparation.
- Dye structure impacted on concentration, stability, and mean size of microbubbles.
- The ratio of albumins to albumin-dye complex in the microbubble structure was approximately equal.
- Microbubble-based fluorescent (Vis, NIR) and US imaging (33, 50 MHz) were demonstrated.

GRAPHICAL ABSTRACT

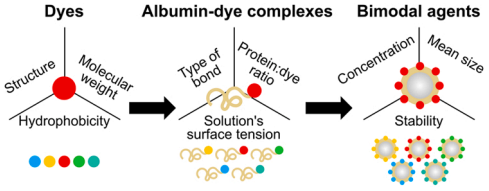

ARTICLE INFO

Keywords:
Gas/liquid interface
Microbubbles
Bovine serum albumin
Fluorescent dyes
Fluorescence imaging
Ultrasound imaging

ABSTRACT

Gas-filled microbubbles are routinely used as ultrasound contrast agents in the clinic. Recently, microbubbles attracted attention as agents for multimodal imaging and image-guided drug delivery. Hence, we prepared microbubbles based on albumin-dye complexes to achieve optimal bimodal (fluorescent/ultrasound) imaging properties. The fluorescent dyes used for *in vitro/in vivo*/medical imaging (Fluorescein, and Rhodamine B, Cyanine 5.5, and Cyanine 7, Indocyanine Green) were introduced into the albumin-dye complex structure. Interconnections between dyes parameters (chemical structure, molecular weight, and hydrophobicity), properties of albumin-dye complexes (type of bond and ratio between protein and dye, solution surface tension), and bimodal agent properties (concentration, mean size, storage stability) were evaluated. Bimodal imaging of "colored" microbubbles was assessed using ultrasound with 33, 50 MHz frequencies and fluorescence

Abbreviations: MBs, microbubbles; US, ultrasound; FL, fluorescent; BSA, bovine serum albumin.

* Corresponding authors.
E-mail addresses: Roman.Barmin@Skoltech.ru (R.A. Barmin), D.Gorin@skoltech.ru (D.A. Gorin).

https://doi.org/10.1016/j.colsurfa.2022.129095
Received 13 October 2021; Received in revised form 24 April 2022; Accepted 25 April 2022
Available online 28 April 2022

tomography. We observed that the ratio between the protein molecules and the protein-dye complex in the microbubble shell was approximately equal, highlighting the impact of dye chemical structure on albumin-dye complex properties and resulting microbubble properties in characterization and imaging. These findings shed light on correlations between microbubble interface stabilization with albumin, microbubble structure formed by albumin-dye complexes, physicochemical properties and applications of bimodal (fluorescent/ultrasound) contrast agents.

1. Introduction

Search for pathological changes in the body at the diseases earliest stage stimulated the development of medical imaging technologies. Hence, ultrasound (US), photoacoustic (PA), and fluorescent (FL) imaging are successfully used in clinical practice [1,2]. The transition from organ to molecular imaging requires combinations of imaging strategies to achieve its synergy, and multimodal imaging has become a recent research hotspot for a detailed analysis of the pathology [1]. Contrast agents with their ability to tune image contrast during the procedure became a point of interest, resulting in the development of multimodal imaging agents [3–7].

US imaging is a workhorse in the clinical routine [8,9]. US includes no radiation, no restrictions on use, simplicity, and low cost of real-time imaging; however, it is an operator-dependent method with moderate contrast resolution [8,10]. Gas-filled microbubbles (MBs) are used in clinics to improve contrast enhancement [11–14]. MBs with the size of 1–7 μm can act as a blood pool agent, where the MB gas core provides acoustic backscattering properties, and the MB shell affects the oscillation properties, agent stability, and circulation time [9,15–18]. In 2016, MBs gained the US Food and Drug Administration approval for non-cardiac contrast, and two targeted MB formulations are under clinical trials for molecular imaging [19,20]. Thus, MBs have already gained the power and expressiveness of routine imaging procedures for faster therapeutic decision-making. Recently developed MB formulations can also contribute to targeted drug delivery (where MB interface is functionalized with therapeutic agents) and multimodal imaging (where MB interface is decorated with inorganic nanoparticles or dye molecules) [21–24].

The choice of shell materials defines the thickness and elasticity properties of the MB gas-liquid interface [9,15–17]. A soft thin lipid shell demonstrates optimal US contrast enhancement, while gas from the core can intensively diffuse, while hard thick polymeric MBs can prevent gas dissolution and increase stability, reducing its contrast enhancement [11,13,14,25]. Thus, the choice of proteins for MB stabilization can compromise soft lipid and hard polymer MB shell properties. Bovine serum albumin (BSA) is considered in recent work for MB preparation due to several reasons: (i) BSA structure and properties are very similar to those of human serum albumin that is present in the blood plasma in sufficient concentration; (ii) commercially available albumin-based agents were pressure-sensitive, hence, there is a need to optimize desired gas-liquid MB interface properties; (iii) albumin itself increases the number of surface groups available for functionalization compared to other MB shell materials [26–33]. Therefore, we focus on BSA-shelled MBs as biocompatible platforms for multimodal agent design.

FL imaging gained applications in cancer research; still, while it is valuable in the preclinical setting, its application to patients is less enforceable [34,35]. In addition, the smart design of bimodal FL, US contrast agents raises the path to high-quality angiography of blood vessels to identify pathologies [34,36,37]. Thus, bimodal imaging agents can benefit from each modality advantages.

Bimodal MBs can be produced with proper interface modification with dyes, and a proper choice of dyes is needed. For example, Fluorescein and Rhodamine are the most frequently used dyes for *in vitro* studies, while *in vivo* imaging requires a shift of absorption/emission peaks in the near-infrared (NIR) spectrum region [38,39]. Indocyanine Green, NIR dye, is already in clinical practice for 50 years and is profitable because of its absorption at the isosbestic point of hemoglobin and oxyhemoglobin spectrum, while the dye may tend to aggregate and interact with plasma proteins, limiting its applicability for use [40–42]. Recently developed NIR cyanine dyes (as Cyanine 5.5 and Cyanine 7) are relevant for *in vivo* imaging purposes; however, undesired aggregation and mild fluorescence in aqueous solution shorten their applications [40,43]. Examples of MBs modified with mentioned dyes are already known in the literature [36,37,44–47]. For example, ICG-functionalized MBs have been involved in bimodal functional imaging of cancer or sentinel lymph nodes localization, while Cyanine 5.5 conjugated MBs composed of chitosan–vitamin C lipid system were addressed tumor-selective *in vivo* imaging [36,46,47]. However, dye incorporation in the MB shell can affect the physicochemical properties of the agent gas-liquid interface, and it was not evaluated for protein-shelled MBs yet. Recently, the incorporation of dyes with variation in hydrophobicity (log P), chemical structure, and molecular weight has shed light on polymer-based MB properties as (model) drug loading and release [48]. Thus, research on BSA MB modification with dyes for bimodal FL/US imaging should consider mentioned dye properties (hydrophobicity, chemical structure, and molecular weight) and their impact on MB FL and US imaging properties.

In this work, we set ourselves to study the incorporation of fluorescent dyes into the gas-liquid interface of BSA-shelled MBs to assess dye impact on MB physicochemical (concentration, storage stability, mean size distribution, dye incorporation efficiency) and bimodal imaging properties. Hence, a set of dyes with different chemical structures, molecular weight, hydrophobicity, and spectral characteristics (excitation/emission pairs, fluorescence quantum yield) was considered: Fluorescein, Rhodamine B, Indocyanine Green Cyanine 5.5, and Cyanine 7. Mentioned dyes were conjugated to BSA for further MB production. MBs were thoroughly assessed to identify optimal bimodal agent structure considering the properties of albumin-dye complexes (surface tension, type of chemical bond, and the number of dye molecules associated with a protein molecule).

2. Materials and methods

2.1. Materials

Bovine serum albumin (BSA), N-Hydroxysuccinimide (NHS), phosphate buffer saline (PBS), dimethylsulfoxide (DMSO), and fluorescent dyes fluorescein-isothiocyanate (FITC), Rhodamine B isothiocyanate (RITC) were all purchased from Sigma-Aldrich (Darmstadt, Germany). Cyanine 5.5 (Cy5.5) N-hydroxysuccinimide ester and Cyanine 7 (Cy7) N-hydroxysuccinimide ester were purchased from Lumiprobe (Hannover, Germany). Indocyanine green (ICG) was purchased from Dynamic Diagnostics (Plymouth, MI, USA). Deionized (DI) water with specific resistivity higher than 18.2 MΩm from a Milli-Q Integral 3 water purification system (Millipore, Burlington, MA, USA) was used to make all solutions.

2.2. Albumin-dye complexes preparation

BSA-FITC and BSA-RITC: BSA (120 mg) was dissolved in 30 mL of phosphate buffer (pH = 8). Then, 4 mg of FITC or RITC were dissolved in a 1:1 DMSO: water mixture with a concentration of 1 mg/mL. The FITC/

RITC solution was poured into the BSA solution with thorough stirring, and the resulting mixtures were stirred for 12 h at a temperature of 4 °C. The resulting complexes were purified by dialysis against deionized water and then were stored at −20 °C.

BSA-ICG: BSA (100 mg) was dissolved in 6 mL of phosphate buffer (pH 7.4) and mixed with 1 mL of ICG solution with a concentration of 7 mg/mL; then, the mixture was stirred for 3 h. The solution was then washed by dialysis against deionized water for 48 h in the cold (4 °C). After dialysis, the solution was diluted twice. The resulting complex was stored at −20 °C.

BSA-Cy5.5 and BSA-Cy7: Bovine serum albumin (120 mg) was dissolved in 30 mL of phosphate buffer (pH 8). Cy 5.5- or Cy7- N-hydroxysuccinimide (NHS) esters were dissolved in DMSO at a 2 mg/mL concentration, respectively. The solution of cyanine esters (Cy5.5 or Cy7, respectively) was poured into the BSA solution with thorough stirring; the resulting mixtures were stirred for 12 h at a temperature of 4 °C. The resulting complexes were purified by dialysis against deionized water and then were stored at −20 °C.

12–14 kDa dialysis membranes (Zellu Trans Dialysis Tube T4, Scienova GmbH, Jena, Germany) were used to purify each albumin-dye complex.

2.3. Mass spectrometry measurements

Samples contained BSA were analyzed using a time-of-flight mass spectrometer with matrix laser desorption/ionization (MALDI-TOF/TOF) rapifleX MALDITOF/TOF MS System (Bruker Daltonik GmbH, Bremen, Germany). The operating mode was as follows: linear mode, positive ionization, analysis range m/z 5000–70000, accelerating voltage 20 kV, SmartBeam III laser, laser frequency 10 kHz, frequency 200 Hz. Before analysis, the device was calibrated using a mixture of proteins, "Protein Calibration Standard I" (Bruker Daltonik GmbH, Bremen, Germany). The mixture included the following proteins: insulin ([M + H] = m/z 5734.5), ubiquitin I ([M + H] = m/z 8565.76), cytochrome C ([M + H] = m/z 12,361.2), myoglobin ([M + H] = m/z 16,952.5). 2.5-dihydroxybenzoic acid (Bruker Daltonik GmbH, Bremen, Germany) with purity > 99.0% was used as the matrix. A 20 mg/mL matrix solution was prepared in a mixture of 30% acetonitrile:70% water:0.1% trifluoroacetic acid. An aqueous solution of the samples was mixed with the matrix in a ratio of 1:1, and 1 μL of the mixture was applied to the target plate.

2.4. Surface tension measurements

Surface tension measurements were obtained using the method described previously [5]. The final result represents the average surface tension and standard deviation of the last 2 min of the 3 repeated measurements.

2.5. Microbubbles preparation

Air-filled MBs were obtained by the modified sonication method [5,30,49]. First, 100 mg of BSA were dissolved in 1 mL of deionized water for each sample. Next, 1 mL of albumin-dye solution (BSA-FITC, BSA-RITC, BSA-ICG, BSA-Cy5.5, BSA-Cy7, respectively) was added to each sample labeled with dyes; or 1 mL of deionized water was added to 1 mL of BSA solution to prepare bubbles with the BSA shell without any additional shell modification. All samples were stored in a glass vial and heated to 50 °C to lower the solution surface tension and prevent protein from denaturation. Next, each sample was sonicated for 3 min at the maximum power of 100 W on the Bandelin Sonopuls HD4100 sonicator with the TS103 sonotrode probe (Bandelin Electronic GmbH & Co KG, Lueneburg, Germany). The tip of the sonotrode was placed at the interface between the phases of liquid solution and air. After sonication, each sample was stored at 4 °C for 30 min for further stabilization.

Next, all samples underwent a dialysis procedure using a 100 kDa dialysis membrane ("Biotech CE Dialysis Tubing 100KD", Repligen Inc., Waltham, MA, USA) to remove free-floating BSA (with a molecular weight of ~67 kDa) and albumin-dye complexes (with a molecular weight of ~67.5–70 kDa) unbound in the MB shell from MB-contained sample, similar to previously described in the literature [5,30]. Dialysis was made at 4 °C for 12 h in saline solution in contact with air.

2.6. Bradford analysis

The Bradford assay analyzed the dialysate of each sample type to evaluate the amount of BSA involved in the bubble shell formation. Briefly, BSA standards in saline ranging from 0.1 to 1.4 mg/mL were prepared for obtaining the calibration curve. First, 5 μL of protein standards were placed into separate wells in a 96-well plate, and to the blank well, 5 μL of saline solution was added. Also, 5 μL of each dialysate with unknown concentrations of BSA were placed in the wells. Then, to each well being used, 250 μL of the previously brought to the room temperature Bradford reagent was added, and the solutions were mixed on a shaker for approximately 30 s. After 5 min of incubation at room temperature, the absorbance was measured at 595 nm using Tecan Infinite M Nano+ (Tecan Trading AG, Männedorf, Switzerland). The BSA concentrations in dialysates were determined according to the standard curve A595 *versus* known concentration. The difference between the solution initial and washed-up BSA amounts were considered the shell-forming protein amount.

2.7. Optical microscopy

Optical microscopy (OM) was carried out on an Olympus CX33 (Olympus Corporation, Tokyo, Japan). In addition, Confocal Laser Scanning Microscopy (CLSM) was carried out on Axio Observer.Z1/7 with Plan-Apochromat 40x/1.3 Oil DIC (UV) VIS-NIR M27 objective (Carl Zeiss Microscopy GmbH, Germany).

Fluorescence lifetime imaging microscopy (FLIM) measurements and image processing were carried out on MicroTime 200 STED microscope (PicoQuant GmBH, Germany), where a 402 nm laser was used as the excitation source, and a 425 nm bandpass filter was applied. Measurements were made at a pulse rate of 40 MHz, a pulse duration of 40 ps, the optical power of 0.4 μW for BSA-FITC MBs samples, and optical power of 3 μW for BSA-RITC MBs samples. Fluorescence lifetime images were acquired in the time domain. The laser beam was focused on MBs with a 100 × 1.4 NA oil immersion objective (UplanSApo, Olympus, Japan). According to the dwell time of 0.4 ms with a pixel size of 0.200 μm, the total image acquisition time was 40 s for an image size of 400 × 400 pixels — 80 × 80 μm.

2.8. Microbubbles size and concentration measurements

The size distribution of MBs was evaluated using images of 200 MBs obtained with OM. MB concentrations were determined with the use of the cell blood counter. For each MB-containing sample, concentrations were determined 30 min after the sonication and (0 h), after storage at 4 °C for 12 h before and after dialysis, and after storage at 4 °C for 36 h and 168 h before and after dialysis. Each measurement was repeated 5 times.

2.9. Dynamic light scattering and zeta-potential measurements

Dynamic light scattering (DLS) and zeta-potential measurements were performed on the ZetaSizer Nano ZS analyzer (Malvern Panalytical, Malvern, UK); all samples were diluted 20 times in deionized water and placed in a U-cuvette. Each measurement was carried out at 25 °C and repeated three times.

2.10. Nanoparticle tracking analysis measurements

Nanoparticle Tracking Analysis (NTA) characterization was performed 1 h after sample preparation. Before analysis, if necessary, to achieve a proper MB concentration, samples were diluted at 1:10 in DI water. The sample was then injected into the test cell and illuminated by a 45-mW blue laser (488 nm wavelength, Nanosight model NS-300, Malvern, Salisbury, UK). The scattered light was video recorded using the built-in high sensitivity sCMOS camera for 60 s at 25 frames per second with 0.1-ms shutter speed. The recording was repeated 5 times for each sample keeping the camera level at 1. Each video consisted of 1498 frames that captured at least 2000 valid particle tracks. The videos were analyzed by NTA software (version 3.2) to evaluate MB size distribution.

2.11. Transmission electron cryomicroscopy (CryoTEM)

For transmission electron cryomicroscopy (CryoTEM) analysis, 3 μL of the sample was placed onto a 200-mesh copper grid covered with lacey film. Grid was previously treated with air plasma. The sample excess was removed by blotting the grid for 1 s and immediately plunged into liquid ethane (automated plunging system, Vitrobot FEI, USA). As a result, a sample was frozen in amorphous ice. Then the sample was transferred in liquid nitrogen to the transmission electron microscope (Tecnai $G^2$12 SPIRIT, FEI, USA).

2.12. Atomic force microscopy

Atomic force microscopy (AFM) images were obtained in tapping mode with the NTEGRA Spectra device (NTMDT-SI, Moscow, Russia) using NSG10 probes (TipsNano, Tallinn, Estonia). The doubled MB shell thickness measurement was performed using a technique similar to [50]. First, the image was flattened as much as possible so that the plane of the substrate became as flat and horizontal as possible. Then, by defining the threshold, the area of the image not covered by objects was selected with a mask (Fig. S1a). The height distribution was calculated for this area, and the maximum distribution was considered the substrate level (Fig. S1b). Then, flat areas on the containers were identified, corresponding to the folded double layer of the MB shell. For this, a range of heights was selected above the substrate but below the folds of the shell protruding above the double layer. The height distribution was again calculated for the masked area (Fig. S1a). The distribution maximum corresponded to the bilayer height, and the distribution width specified the thickness variability (Fig. S1b). Finally, the substrate height was subtracted from the bilayer height to determine the MB shell thickness, and the resulting value was divided by two.

2.13. Scanning electron microscopy

Scanning electron microscopy (SEM) images were obtained with scanning electron microscope MIRA II LMU (Tescan Orsay Holding, Brno, Czech Republic). Samples were prepared by depositing a drop of MB suspension on a silicon wafer and drying at room temperature (25 °C). Then, dried specimens were sputter-coated with approximately 5 nm thick gold film using a Denton sputter-coater before SEM.

2.14. Extinction spectra measurements

Extinction spectra were measured using a Tecan Infinite M Nano+ reader (Tecan Trading AG, Männedorf, Switzerland) at room temperature (25 °C), where samples were placed in a plastic 96-well plate. All samples were diluted 1, 2, 4, 8, 16, 32, 64, 128, 256 times compared with the initial concentration in deionized water for one set of experiments and with concentrations of 1×10^8, 5×10^7, 2.5×10^7, 1.2×10^7, 6.5×10^6 MBs/mL for another set of experiments.

2.15. Method for the determination of dye concentrations

The used albumin-dye complexes were diluted 1, 2, 4, 8, 16, 32, 64, 128, 256 times compared with the initial concentration in DI water, then the extinction spectra for each albumin-dye sample were obtained. In addition, the extinction spectra were measured for the tater obtained after MB-containing samples dialysis. Then, linear calibration curves were constructed for the extinction values for each type of the albumin-dye complex solution. Then the fractions of fluorescent complexes included in the MB shell structure were calculated for each type of sample (BSA-FITC, BSA-RITC, BSA-ICG, BSA-Cy5.5, and BSA-Cy7).

2.16. Flow cytometry measurements

Flow cytometry experiments were performed with the CytoFLEX system (Beckman Coulter, Brea, CA, USA), equipped with three excitation sources (405, 488, and 635 nm). FITC-A channel was used for BSA-FITC MBs sample analysis, PE-A channel was used for BSA-RITC MBs sample analysis, APC-A750-A channel was used for BSA-Cy5.5 MBs sample analysis, PC7-A channel was used for BSA-ICG MBs and BSA-Cy7 MBs samples analysis, respectively. All samples were diluted 1000 times, and 500–1000 events were recorded for each sample.

2.17. Fluorescence tomography measurements

For FL tomography measurements, each sample was diluted in saline and added to a 96-well plate in the same manner as for extinction spectra measurements. The plate with samples was then imaged by the IVIS CT Spectrum In Vivo system (Xenogen Corp., San Francisco, CA, USA) at body temperature (37 °C). Sequence images were acquired with the following Excitation/Emission pairs: the pair of 500/540 nm for samples containing FITC, the pair of 535/580 nm for samples containing RITC, the pair of 745/840 nm for samples containing ICG, the pair of 675/720 nm for samples containing Cy5.5, the pair of 745/840 nm for samples containing Cy7. Photons were quantified with the LivingImage software v.4.5.3 (Xenogen Corp., Alameda, CA, USA).

2.18. Acoustic characterization

The DUB® SkinScanner (Taberna Pro Medicum GmbH, Lueneburg, Germany) was used to evaluate US contrast of MBs at frequencies of 33 MHz and 50 MHz. The received signals were processed using DUB SkinScanner software v.5.31 (Taberna Pro Medicum GmbH, Lueneburg, Germany). Samples were tested 12 h after preparation without dialysis; all measurements were carried out at body temperature (37 °C).

3. Results and discussion

3.1. Formation of gas-liquid interface with albumin-dye complexes: choice of dyes, formation of albumin-dye complexes, and evaluation of protein packing in the gas-liquid interface of microbubble shell

A set of FL dyes is considered for MB modification in the presented work: Fluorescein and Rhodamine B are classical dyes for *in vitro* imaging [38], while Cyanine 5.5 and Cyanine 7 are recently-developed *in vivo* molecular imaging dyes [40]. In addition, Indocyanine Green is used due to its long history of use in medical imaging and recent applications in PA imaging [41,42]. A comparison of both chemical (molecular weight, hydrophobicity) and optical (relevant excitation/emission pairs, FL quantum yield) properties for described dyes is presented in Table 1. A wide range of dyes opens the possibility of operation at different wavelengths in the visible and NIR spectrum range for bimodal MBs.

Next, albumin-dye complexes are prepared to uniform the procedure of dye loading in the MB shell. The stitching structures are presented in Fig. S2: the crosslinking between BSA and dye molecules is confirmed

Table 1
Overview of the fluorescent dyes used in the presented work: molecular weight, hydrophobicity [51–54], excitation/emission wavelengths pairs [55–59], fluorescence quantum yields [55–59], and current biomedical applications [38,40,41].

Dyes	Molecular weight (Da)	Hydrophobicity (log P)	Excitation / emission pair (nm)	Fluorescence quantum yield (units)	Applications
Fluorescein ($C_{20}H_{12}O_5$)	332.31	3.35	495/520	0.93	*In vitro* imaging
Rhodamine B ($C_{28}H_{31}ClN_2O_3$)	479.01	1.95	570/595	0.65	*In vitro* imaging
Indocyanine Green ($C_{43}H_{47}N_2NaO_6S_2$)	775.0	-0.29	789/814	0.03	Medical imaging
Cyanine 5.5 ($C_{40}H_{43}N_2O_2+$)	583.33	4.94	675/694	0.2	*In vivo* imaging
Cyanine 7 ($C_{37}H_{45}N_2O_2+$)	549.35	-3.74	753/775	0.3	*In vivo* imaging

using mass spectrometry measurements. Thus, the crosslinking is carried out covalently for a set of dyes except for Indocyanine Green (Fluorescein, Rhodamine, Cyanine 5.5, Cyanine 7). Indocyanine Green tends to bind with a protein electrostatically. Mass-spectrometry measurements are presented in Fig. S3.

To produce MBs stabilized by albumin-dye complexes, initial solutions are prepared to keep the mass concentration of protein around the optimal value of 5% [5,60]. Briefly, 1 mL of pure protein solution (with protein mass concentration of ~10%) was mixed with 1 mL of albumin-dye complex aqueous solution (with protein mass concentration of ~0.2–0.3%); thus, the resulting protein mass concentration should be ~5%.

Next, the surface tension value is measured for each initial "colored" solution. Fig. 1 demonstrates that the value of the dye hydrophobicity is inversely proportional to the value of the solution surface tension for the corresponding albumin-dye complex. In other words, the higher the hydrophobicity expected for the dye, the lower value of the surface tension is observed for the "colored" solution used for MB preparation. Furthermore, introducing the dye in each complex lowered solution surface tension compared to 5% BSA aqueous solution (with the value of 54.1 ± 0.3 mN/m).

MBs are produced using the method presented in Fig. 2a [5,61,62]. The optimal conditions for stable samples preparation are US power of 100 W, sonication for 3 min, and the sonotrode tip location at the air-liquid interface. The temperature of the solution is raised to 50 °C for two reasons: (i) to reduce the surface tension of the initial solution and produce MBs with narrow size distribution and (ii) to prevent albumin from denaturation during the MB synthesis. After preparation, MB-containing solutions are stored in the fridge (4 °C) for 30 min for MB stabilization.

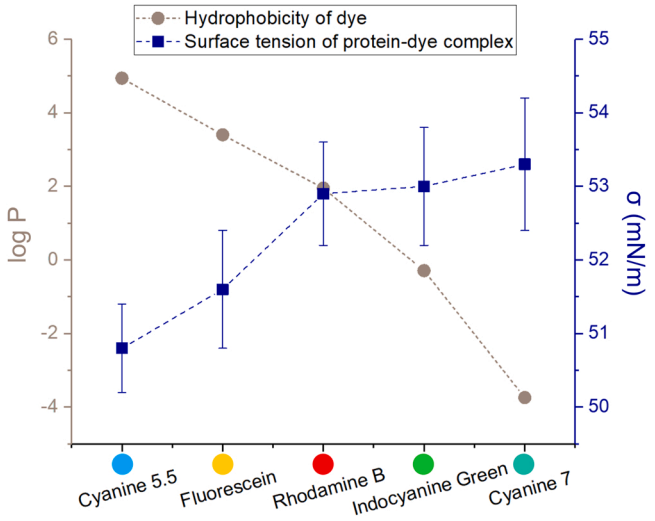

Fig. 1. Correlation between dye hydrophobicity (log P) and surface tension (σ, mN/m) of initial "colored" solutions used for MB preparation, where albumin-dye complexes are introduced.

A series of MBs filled with air is considered in the manuscript: MBs with the shell consisted of BSA only (BSA MBs), and MBs with the shell functionalized with Fluorescein (BSA-FITC MBs), Rhodamine B (BSA-RITC MBs), Indocyanine Green (BSA-ICG MBs), Cyanine 5.5 (BSA-Cy5.5 MBs) and Cyanine 7 (BSA-Cy7 MBs), respectively, using prepared albumin-dye complexes. The presence of free components in these solutions that are not bound to the MB shell leads us to introduce the final step of MB preparation – the dialysis using a 100 kDa dialysis membrane against deionized water fridge conditions (4 °C) for 12 h to remove free components with a molecular weight of 67–70 kDa [61]. The OM images of BSA-RITC MBs and BSA-ICG MBs can be seen in Fig. 2b and c.

A fascinating question is: how do protein molecules (like, in our case, albumin) should form an MB interface? Suppose the MB shell consists of protein globules. Thus, the ratio of the number of protein molecules presented in the initial solution to form one bubble to the number of protein molecules required for the shell formation can be assumed, as described in Equations S1-S5. Therefore, for the assumption when protein was considered as globule, it turns out that there are 2.9×10^5 BSA globules are incorporated into each MB, while the synthesis procedure initially takes ~1550 times more molecules per bubble, as calculated from Equation S5. Another estimation is considered, assuming that the BSA molecule has the shape of an ellipsoid with dimensions 14 nm × 4 nm × 4 nm [63]. Corresponding calculations (presented in Equations S6-S8) turn out that there are 5.7×10^4 BSA globules are incorporated into each MB, and the synthesis procedure initially requires even ~7890 times more molecules per MB.

Next, the following experiment is carried out to assess the correctness of mentioned assumptions. As described above, the second stage of the MB production method is purifying the samples by dialysis with the 100 kDa dialysis membrane. Therefore, counter solutions after the dialysis procedure can be collected, and quantitative analysis can be performed by the Bradford method for protein concentration. Therefore, we can determine the amount of unbound albumin washed out of the system with the mentioned steps (counter solutions collection and the Bradford method analysis). Furthermore, the dye concentration in the counter solution is evaluated for each dye using spectrophotometric analysis and the amount of the dye inside each MB sample. Thus, the calculations of the total number of BSA molecules per one MB and the number of molecules of the BSA-dye complex molecules of the pure BSA in one MB are shown in Table S1.

Thus, it turns out that the first assumption about the invariability of the protein tertiary structure is incorrect. According to the literature, we can assume that prolonged sonication promotes the opening of the

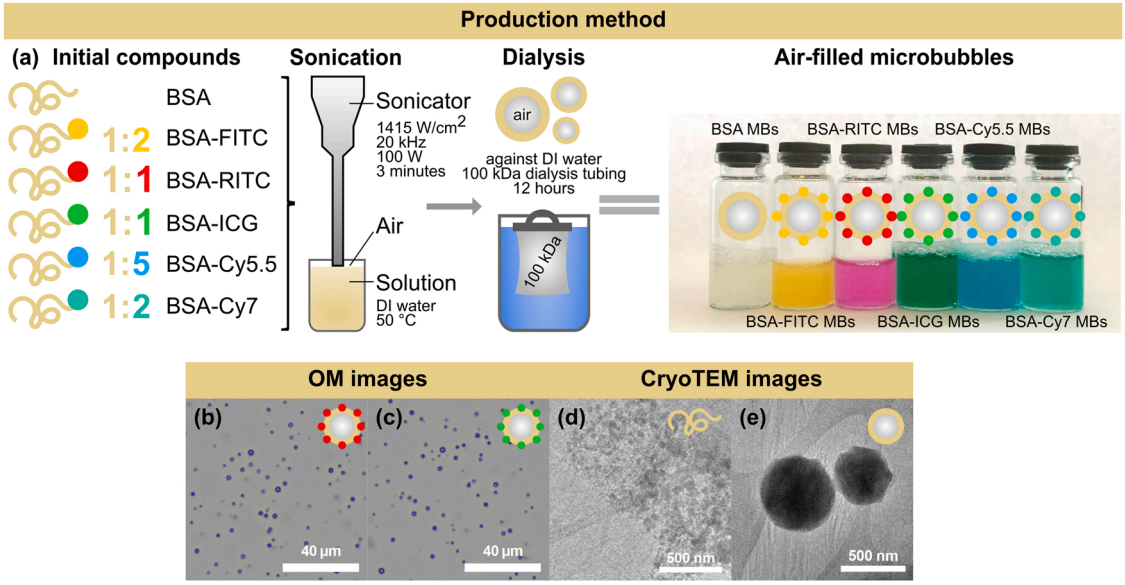

Fig. 2. (a) Scheme of MB production by sonication method: BSA is used as the main component for the shell preparation, and albumin-dye complexes of BSA with fluorescent dyes, Fluorescein (BSA-FITC), Rhodamine (BSA-RITC), Indocyanine Green (BSA-ICG), Cyanine 5.5 (BSA-Cy5.5) and Cyanine 7 (BSA-Cy7) are used for MB modification. All compounds were dissolved in deionized water and then obtained solutions were sonicated for 3 min to produce MBs. After preparation, MBs were dialyzed in deionized water to remove free components from the solution. The resulting MBs are filled with air and stabilized with BSA shell (BSA MBs), or each albumin-dye complex shell (BSA-FITC MBs, BSA-RITC MBs, BSA-ICG MBs, BSA-Cy5.5 MBs, BSA-Cy7 MBs, respectively); (b–c) Optical microscopy (OM) images of (b) BSA-RITC MBs and (c) BSA-ICG MBs; (d–e) Transmission electron cryomicroscopy (CryoTEM) images of (d) BSA molecules and (e) BSA MBs.

tertiary structure, the formation of new hydrophobic and electrostatic bonds, and possibly ordered dense protein chains [64–66]. The results presented in Table S1 show that the number of protein molecules required to form one MB is ~107 and differs by two orders of magnitude, comparing the previously calculated value of ~10^5 with the assumption that protein remained as globules/ellipsoids. This difference between assumptions and experimental data indicates a change in the tertiary structure of proteins and a denser packing of molecules with the formation of hydrophobic, hydrogen, electrostatic, and covalent bonds.

Unfortunately, it is difficult to experimentally confirm the protein structure in MB shell structure due to the fragility of MBs [67–69]. Therefore, cryomicroscopy is a suitable method for confirming the shell structure formed by proteins without MB destruction. CryoTEM measurements are demonstrated in Fig. 2 and confirm our assumption. Images of BSA molecules and BSA MBs are demonstrated (Fig. 2d and e): MB shell remained a smooth flat surface presented in Fig. 2e, without including any separate globules in the structure of the bubble (globules are presented in Fig. 2d). It correlates with the literature-known examples, where a smooth flat surface of a BSA shell without any inclusions was observed [70]. The difference in obtained images contrast (Fig. 2d and e) is observed due to the sample density difference, caused by a possible packing of proteins change within the MB shell structure.

Furthermore, despite the initial predominance of pure protein molecules in initial solutions, the MB shell structure enters an approximately equal ratio between the protein molecule and the albumin-dye complex for "colored" MBs, as demonstrated in Fig. 3. The advantage of the

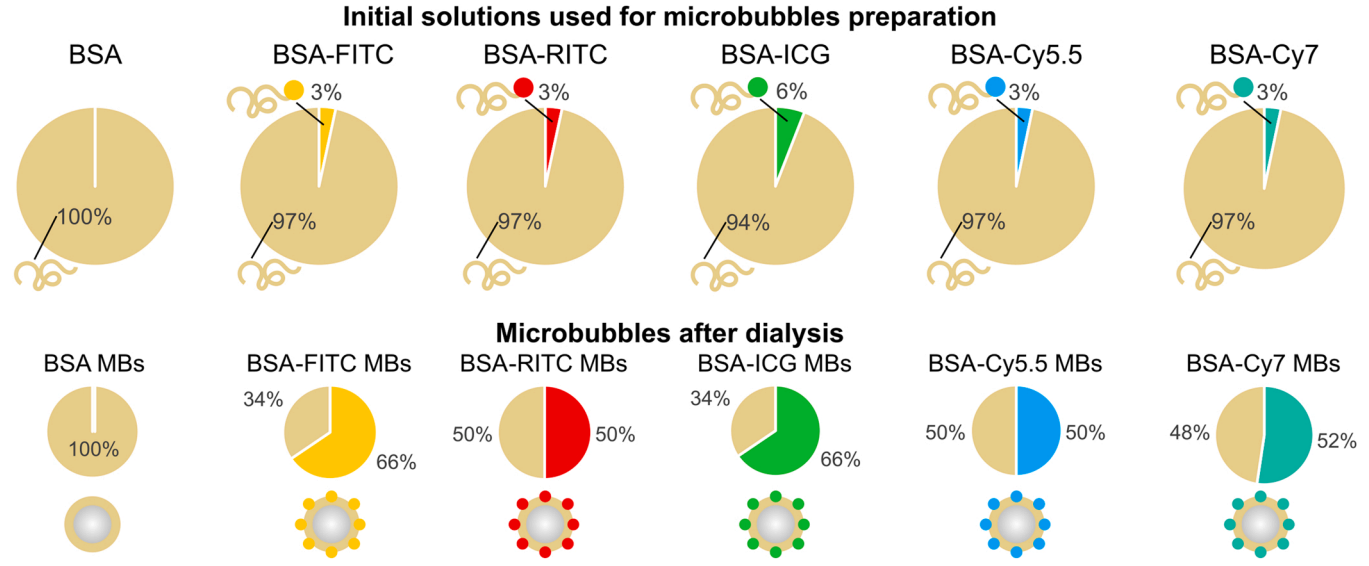

Fig. 3. The ratio of protein and albumin-dye complex for initial solutions used for MB preparation (upper panel, total protein mass concentration is ~5%) and the ratio of protein and albumin-dye complex for the shell of produced MBs after dialysis (lower panel, total protein mass concentration is ~0.2–0.3%).

"colored" albumin-dye complex compared with the pure protein in MB shell formation can be explained by changing of hydrophobicity of the dye-protein complex. The dye introduces a hydrophobic component into the protein structure and the MB interface. A pronounced hydrophobic fragment allows the molecule to integrate into an MB interface more efficiently.

As presented in Table S1, there are from 4.6×10^7 to 23.0×10^7 total protein molecules per one MB shell for "colored" MBs. Also, the value of protein molecules needed for the shell formation increases with the dye hydrophobicity (log P).

Thus, crosslinking of dyes with different chemical (*i.e.,* hydrophobicity) and optical properties with protein is carried out covalently (for Fluorescein, Rhodamine, Cyanine 5.5, Cyanine 7) and electrostatically (for Indocyanine Green). As a result, the introduced dye hydrophobicity (*log P*) is inversely proportional to the value of the surface tension of the solution containing each albumin-dye complex. Furthermore, it is demonstrated that: (i) a change in the tertiary structure of proteins and a denser packing of molecules took its place during the US-assisted formation of the MB shell and confirmed by calculations and TEM images (Fig. 2e), (ii) ~ 10^7 total protein molecules are needed for the formation of one MB, and increasing dye hydrophobicity (log P) will lead to increase in the number of molecules needed for shell formation, and (iii) despite the initial predominance of pure protein molecules in the solutions used for samples preparation, the bubble structure enters an approximately equal ratio between the protein molecule and the albumin-dye complex. Then, with gained knowledge on MB interface formation, physicochemical characterization for each sample is needed.

3.2. Physicochemical parameters of microbubbles: concentration, mean size, and stability

For "colored" MBs assessment, physicochemical parameters of MBs (concentration and size distribution) should be evaluated first. Then, several methods can be used: dynamic light scattering (DLS), nanoparticle tracking analysis (NTA), and optical microscopy (OM). Hence, the results are presented in Table S2. As one can see, obtained results slightly differed; however, the trend in agent sizing persisted for different samples remained the same. Therefore, OM data is the most objective tool beyond the other mentioned methods.

Thus, the concentration of MBs was determined by two methods: OM (using a cell blood counter) and NTA. The obtained data differed in absolute values but had the same trend presented in Fig. 4**.** The difference in values can be described considering detection limits for both methods. The resolution of OM does not allow detecting objects less than 500 nm, while NTA does not consider objects above 1 μm. Respectively, some MBs (in this case, more significant than 1 μm) cannot be considered by NTA measurements, while the tiniest MBs cannot be adequately detected using OM. However, both methods (NTA and OM) were applicable for concentration measurements of MBs. Therefore, OM is chosen to evaluate MB concentration and storage stability.

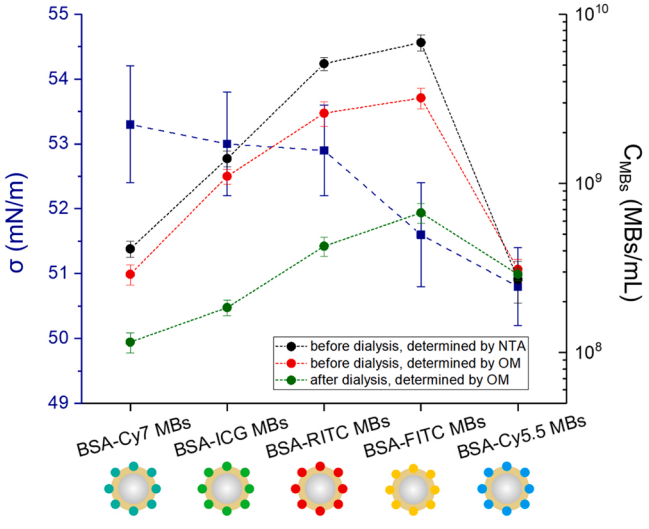

Fig. 4. Correlation between surface tension (σ, mN/m) of initial solutions used for MB preparation (blue line and dots) and concentrations of produced MBs (C_{MBs}, MBs/mL), calculated using NTA (black line and dots) and OM measurements (red line and dots) for samples before dialysis, and calculated using OM measurements (green line and dots) for samples after dialysis.

According to Laplace pressure, the modulus of pressure difference is proportional to the surface tension of the interface between liquid and gas. In other words, it is expected that with the lower value of the surface tension of the initial solution used for MB preparation, a lower pressure difference should affect MB compression. Hence, a lower pressure difference should result in a higher initial concentration of MBs in the sample and prolonged stability against gas exclusion from the MB gas-liquid interface.

Interestingly, Fig. 4 shows no direct relationship between the initial solution surface tension and the resulting MB concentrations. It can be explained by the impact of albumin-dye complexes introduction in MB preparation: the structure of the albumin-dye complex used for each sample preparation (type of bond between protein and dye, protein: dye ratio) should play its role in affecting MB concentration and stability properties. The impact of albumin-dye complexes is more significant than solution surface tension when dyes are coupled with protein.

Next, the concentration for each sample was evaluated with a cell blood counter using OM during storage time, as one can see in Fig. S4. Time points of 1, 12, 36, and 168 h after preparation are considered for samples without dialysis, and points of 12, 36, and 168 h after preparation are considered for dialyzed samples. All samples were stored at the same temperature (4 °C).

In ascending order of the MB concentration immediately after preparation, the samples can be arranged as follows: BSA-Cy7 MBs (7.4×10^8 MBs/mL), BSA-Cy5.5 MBs (7.6×10^8 MBs/mL), BSA MBs (1.8×10^9 MBs/mL), BSA-ICG MBs (2.0×10^9 MBs/mL), BSA-RITC MBs (5.1×10^9 MBs/mL), BSA-FITC MBs (1.1×10^{10} MBs/mL). The dye inclusion in the MB shell increased the initial concentration of MBs compared to BSA MBs for Fluorescein, Rhodamine, and Indocyanine Green, as shown in Fig. S4a–d. At the same time, Cyanine 5.5 and Cyanine 7 tend to decrease the initial MB concentration compared with shells consisting of pure BSA (Fig. S4e and f). Then, during storage time, samples without dialysis tended to decrease their concentration after storage for 12 h compared with concentrations after preparation: BSA MBs, BSA-RITC MBs, and BSA-ICG MBs samples demonstrated higher stability and reduced their concentration by less than two times (1.51, 1.98 and 1.78 times, respectively), while less stable samples functionalized with Fluorescein, Cyanine 5.5 and Cyanine 7 reduced their concentration by 3.3 times for BSA-FITC MBs, 2.58 times for BSA-Cy5.5 MBs and 2.53 times for BSA-Cy7 MBs. This observation can demonstrate the impact of the chemical structure of the initial fluorophore and albumin-dye complex properties on "colored" MB formation.

Dialysis using a 100 kDa dialysis membrane removed impurities and free components that are not bound in the MB shell. However, mechanical effects during dialysis may affect on stability and concentration properties of samples. In ascending order of the MB concentration after dialysis for 12 h, the samples can be arranged as follows: BSA-Cy7 MBs (with a concentration of 1.2×10^8 MBs/mL), BSA MBs (1.6×10^8 MBs/mL), BSA-ICG MBs (1.8×10^8 MBs/mL), BSA-RITC MBs (4.3×10^8 MBs/mL), BSA-Cy5.5 MBs (3.9×10^8 MBs/mL), BSA-FITC MBs (6.7×10^8 MBs/mL). Still, the trend of stability and samples concentrations remained the same as for samples without dialysis. BSA MBs, BSA-RITC MBs, and BSA-ICG MBs samples demonstrated higher stability and reduced their concentration by less than 1.3 times (1.21, 1.27, and 1.26 times, respectively), comparing concentrations at 12 and 36 h after MBs preparation, while BSA-FITC MBs sample reduced its concentration by

4.16 times. A similar trend was observed one week after MB preparation: "colored" samples after dialysis BSA-RITC MBs and BSA-ICG MBs demonstrated higher concentrations than pure BSA MBs sample (1.54×10^8 MBs/mL, 1.24×10^8 MBs/mL, and 1.21×10^8 MBs/mL, respectively). Thus, (i) the impact of the chemical structure of the initial fluorophore on "colored" MBs formation is significant, (ii) samples functionalized with Rhodamine (BSA-RITC MBs) and Indocyanine Green (BSA-ICG MBs) demonstrate higher stability during storage than pure albumin-shelled BSA MBs, thus, can be considered as optimal in the described set of "colored" MBs.

Mean size distributions are calculated at 12 and 168 h after sample preparation for all obtained samples using OM images. Images for all produced samples 12 h later preparation are demonstrated in Fig. S5. All MB-containing samples had a submicron- and micron- size range: for samples treated without dialysis, the largest mean size was observed for BSA-ICG MBs (1.0 ± 0.7 μm), and the lowest one was observed for BSA MBs (0.7 ± 0.4 μm). However, samples without dialysis demonstrate the presence of "giant" bubbles (especially the BSA-FITC MBs sample). Also, OM and mean size measurements for samples 168 h after preparation can be seen in Fig. S6, presenting a further slight increase in mean size distributions. However, after dialysis, BSA-RITC MBs and BSA-ICG MBs demonstrate similar size distributions at 12 and 168 h, as evidence of these samples' optimal stability.

The zeta potential of all MB-containing samples showed moderate stability. For BSA MBs, BSA-RITC MBs, and BSA-ICG MBs, stability was revealed up to 47 days under storage conditions, as demonstrated in Table S3.

Therefore, the optimal MB samples are MBs functionalized with Rhodamine B (BSA-RITC MBs) and Indocyanine Green (BSA-ICG MBs), as supported by Fig. S4, Tables S2, and S3. Further evaluation of BSA-RITC MBs and BSA-ICG MBs samples is presented in Fig. 5, with the results of CLSM presented in Fig. 5a and d, AFM measurements presented in Fig. 5b and e, and SEM images of dried samples presented in Fig. 5c and f, respectively.

Using AFM measurements (Figs. 5b and e, S1), we calculated the shell thickness of ~20–30 nm (20.7 ± 5.0 nm for BSA-ICG MBs and 33.5 ± 3.4 nm for BSA-RITC MBs). These results correlate with the shell thickness of commercially-available albumin-based agent, Albunex (Molecular Biosystems Inc., San Diego, CA), where thickness range from 15 to 50 nm was demonstrated [71–74].

Additionally, the stability of produced "colored" MBs is investigated by SEM measurements. The resulting images for BSA-RITC MBs and BSA-ICG MBs are presented in Fig. 5c and f (while SEM images for all "colored" MBs can be seen in Fig. S7). The selected technique is suitable for dried MB morphology assessment without the need for cryomicroscopy of MB-containing samples [65,75–78]. Suspensions of MBs were stable enough to retain spherical morphology and air inside the core even after drying [33].

Therefore, all described samples of MBs stabilized with fluorescent dyes had parameters of size distributions and concentrations that meet optimal US contrast agent criteria. However, the following observations are highlighted: (i) the impact of the chemical structure of the initial fluorophore on "colored" MB concentration and further stability is observed; (ii) samples functionalized with Rhodamine (BSA-RITC MBs) and Indocyanine Green (BSA-ICG MBs) are chosen as optimal due to their stability properties up to 47 days (Table S3), significant concentration values over time (Fig. S4), and narrow size distributions. Next, evaluation of dye incorporation in the MB shell and bimodal FL/US imaging properties will be discussed.

3.3. Evaluation of the efficiency of incorporation of fluorescent dyes into the shell

Two spectrophotometric methods, flow cytometry and fluorescence lifetime imaging microscopy (FLIM), are considered to evaluate the efficiency of dye incorporation into the MB shell structure.

After the agent preparation, both the pure protein and the albumin-dye complex are washed out during dialysis with a 100 kDa dialysis membrane. From the set of experiments and calculations presented in Section 3.1, it is demonstrated that, in general, the pure protein is washed out in much more significant quantities than the albumin-dye complex, which suggests that the amphiphilic albumin-dye structure can be considered as favorable for MB structure formation, comparing with the pure protein structure. Extinction spectra measurements of MBs

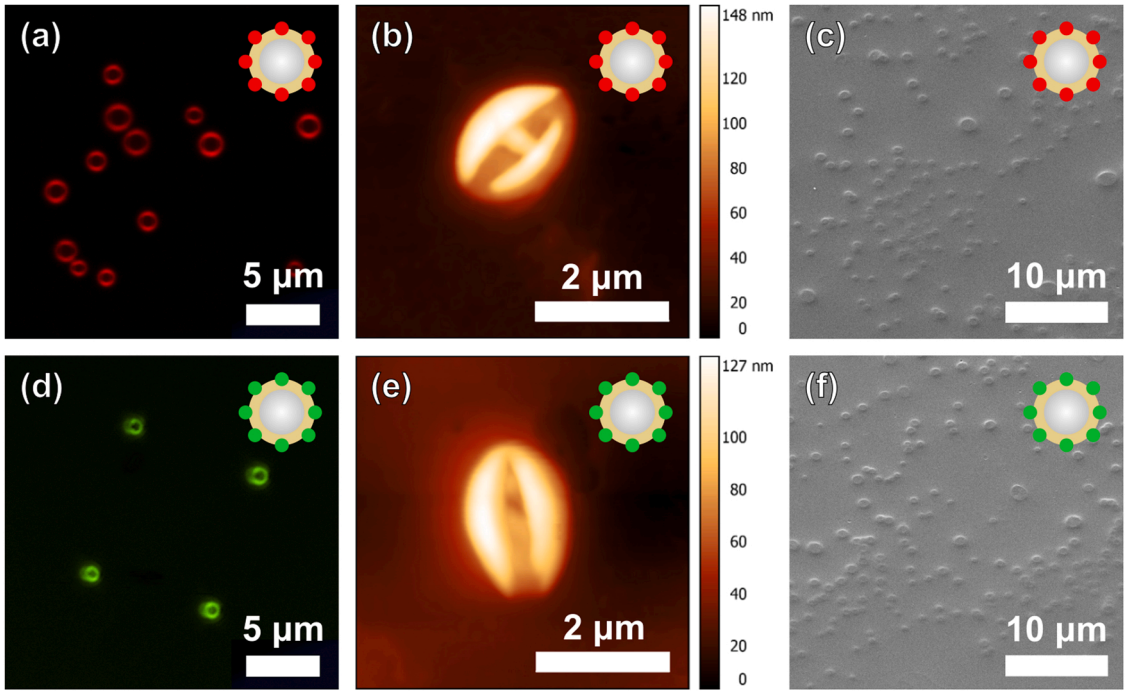

Fig. 5. Optimal MB samples functionalized with fluorescent dyes: (a) OM, (b) CLSM, and (c) SEM images for BSA-RITC MBs, and (d) OM, (e) CLSM, and (f) SEM images for BSA-ICG MBs.

after dialysis in the same agent concentrations confirmed the presence of dye in a considerable amount within the MB structure for each presented sample, as demonstrated in Fig. S8. Next, to determine the presence of MBs containing fluorescent dyes in the shell after dialysis treatment, flow cytometry measurements were obtained for each "colored" MB sample, as shown in Fig. 6.

As one can see, 91% of BSA-FITC MBs included Fluorescein dye in the bubbles shell; 89% of BSA-RITC MBs included Rhodamine dye in the shell; 86% of BSA-Cy7 MBs included Cyanine 7 dye in the shell, and 67% of BSA-ICG MBs included Indocyanine Green dye in the shell; while only 56% of BSA-Cy5.5 MBs included Cyanine 5.5 dye in the MB shell. Still, the fluorescence quenching process can occur during the flow cytometry measurements, comparing these results with the calculations presented above: the albumin-dye complex quenching may occur due to the stacking of dye molecules in a tight package formed during MB synthesis. In samples with a high albumin-dye ratio (as BSA-Cy5.5, with the ratio of 1:5), quenching is more pronounced; thus, we can conclude that the ratio of protein: dye as 1:1 is more favorable than higher amounts of dye to prevent fluorescence quenching.

For samples containing Fluorescein and Rhodamine B, it was possible to obtain FLIM. Thus, FLIM images of corresponding samples (BSA-FITC MBs and BSA-RITC MBs) are presented in Fig. S9a and b, respectively. The FL lifetime distribution heterogeneity is observed during the experiment for solutions of the albumin-dye type complexes and corresponding "colored" MBs. For Fluorescein-contained samples, the average FL lifetime for the albumin-dye complex (BSA-FITC) is 1.55 ± 0.01 ns, while BSA-FITC MBs have an average fluorescence lifetime of 2.46 ± 0.19 ns. Similarly, the average FL lifetime for the BSA-RITC complex is 1.61 ± 0.02 ns, while BSA-RITC MBs have an average fluorescence lifetime of 2.11 ± 0.15 ns. It can be explained in the following manner. The formation of the dye microenvironment in MB shell structure differs from the dye microenvironment in the solution. This effect contributes to an increase in the FL lifetime with a change in the polarity of the solution relative to the polarity of the microenvironment inside MBs. Additionally, this hypothesis can be validated by correlations of the MB size with the fluorescence lifetime, which occurred for BSA-FITC MBs and BSA-RITC MBs samples, as demonstrated in Fig. S10 [49,79,80].

Thus, the inclusion of various fluorescent dyes into the shell structure is confirmed using a set of methods.

3.4. *Fluorescent and ultrasound imaging characterization of produced microbubbles*

Next, bimodal imaging applications of MBs are tested. The results of the FL tomography measurements depending on dye concentration are presented in Fig. 7. Comparison of the dependences of the total radiation efficiency on the concentration of dye molecules is demonstrated for initial solutions used for samples preparation, the resulting solutions containing MBs before dialysis with the presence of albumin-dye complexes in the environment (12 h after preparation without dialysis, samples were stored at a temperature of 4 °C); as well as solutions of MBs after additional dialysis using 100 kDa membrane in the absence of unbound albumin-dye complexes in solution for 12 h stored at a temperature of 4 °C.

Black lines correspond to solutions used for MB preparation

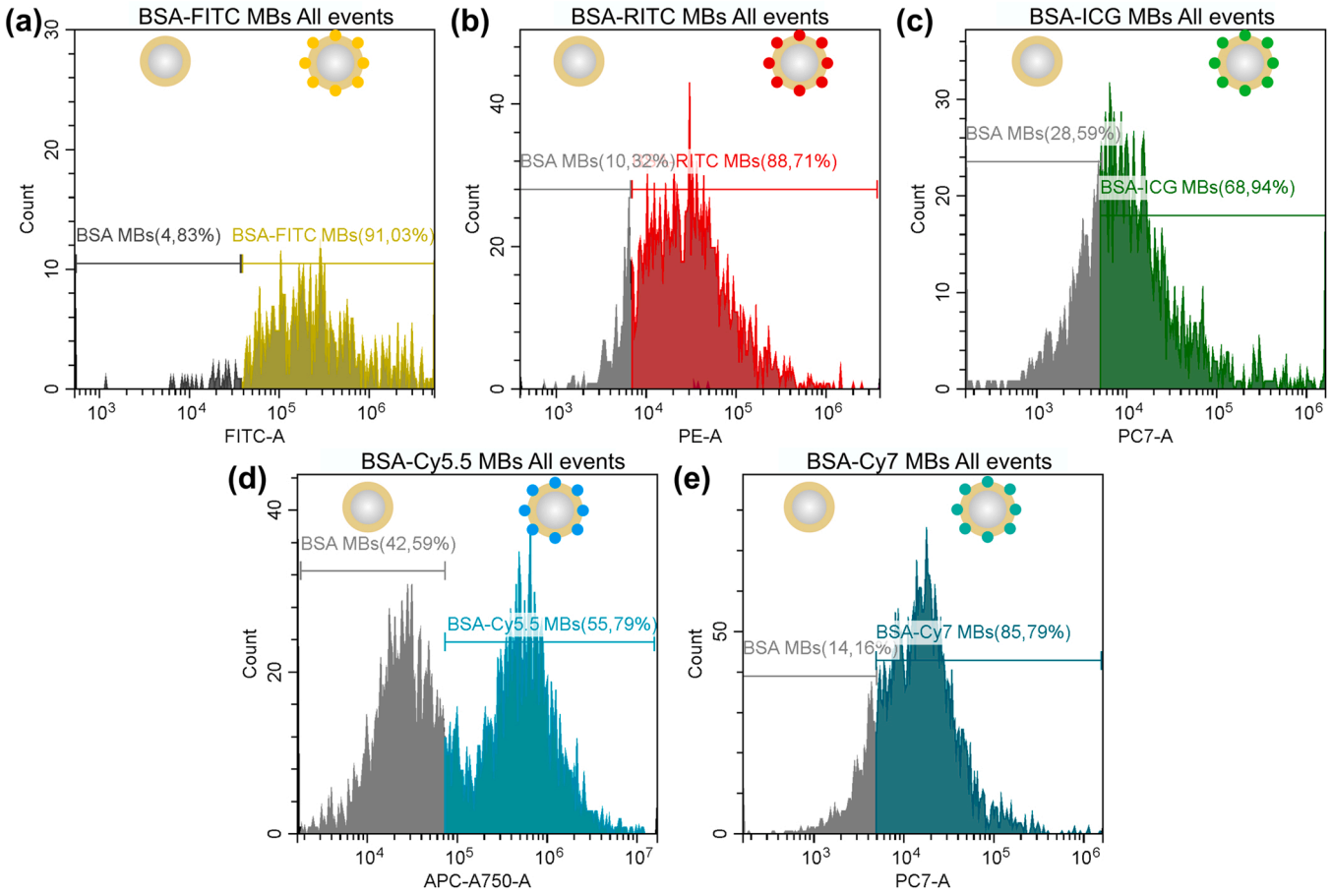

Fig. 6. Flow cytometry measurements for MBs contained fluorescent dyes in the shell structure: (a) Fluorescein (BSA-FITC MBs), (b) Rhodamine B (BSA-RITC MBs), (c) Indocyanine Green (BSA-ICG MBs), (d) Cyanine 5.5 (BSA-Cy5.5 MBs), (e) Cyanine 7 (BSA-Cy7 MBs), compared with BSA MBs, to determine the amount of "colored" MBs with the dye included in the shell. FL parameters for each measurement were considered according to Table 1 of the manuscript.

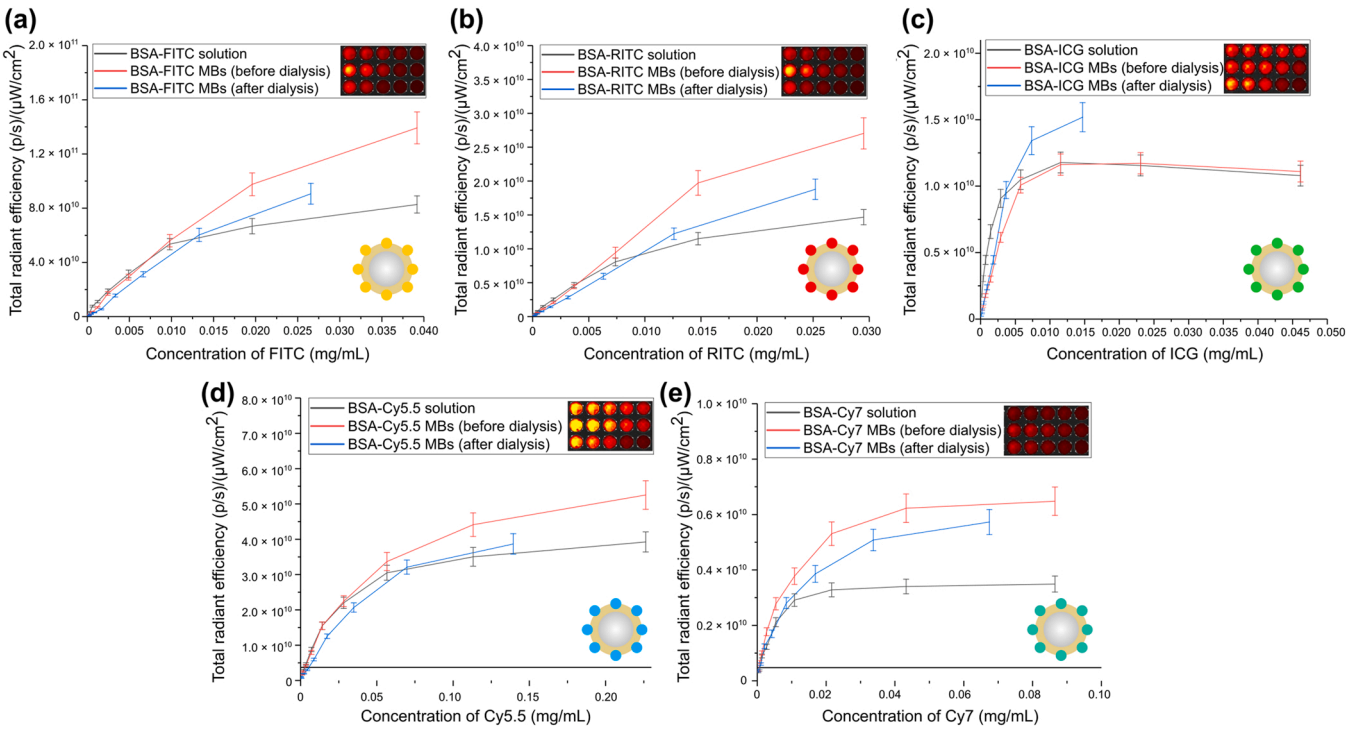

Fig. 7. Fluorescence tomography measurements: comparison of total radiant efficiency dependencies on the dye concentration for (a) Fluorescein, (b) Rhodamine B, (c) Indocyanine Green, (d) Cyanine 5.5, (e) Cyanine 7.

containing relevant albumin-dye complexes; blue lines correspond to MB-containing samples before dialysis; red lines correspond to MB-containing samples after dialysis. Inlets on each figure show FL imaging of a plate with corresponding samples presented in each Figure.

For all the samples (except for the samples containing Indocyanine Green), an increase in the FL signals of the solution is observed after MB introduction compared with the initial solution. The presence of MBs in the sample and significant internal light reflections inside the air core of MBs led to a significant increase in the FL signal 1.34–1.86 times compared to initial solutions. A high dye concentration of solution samples containing free Indocyanine Green molecules resulted in FL quenching. The corresponding concentration of FL quenching is observed with a concentration of Indocyanine Green higher than 0.02 mg/mL, which correlates with previous reports [81]. However, for all MBs samples after dialysis, the fluorescent signal obtained only from MBs was higher than for initial solutions used for MB preparation; thus, these concentrations can be considered optimal for the use of presented purified "colored" MBs as contrast agents for FL tomography. Also, the dependences of the total radiation efficiency on the concentration of MBs after dialysis were identical to the dependences obtained for MBs before dialysis for each type of albumin-dye complex used for sample preparation. For MB-containing samples before and after dialysis, the highest total radiant efficiency values were observed for the Fluorescein-contained sample (BSA-FITC MBs); other samples can be arranged in descending order for samples contained: Cyanine 5.5 (BSA-Cy5.5 MBs), Rhodamine B (BSA-RITC MBs), Indocyanine Green (BSA-ICG MBs), and Cyanine 7 (BSA-Cy7 MBs), respectively.

The FL tomography measurements depending on MB concentration are also presented in Fig. S11. In terms of FL signal efficiency, the samples could be ranked from highest to lowest in the following order for samples containing Fluorescein (BSA-FITC MBs), Cyanine 5.5 (BSA-Cy5.5 MBs), Indocyanine Green (BSA-ICG MBs), Rhodamine B (BSA-RITC MBs), Cyanine 7 (BSA-Cy7 MBs). In contrast, the sample containing pure protein only in the shell (BSA MBs) demonstrates a lack of FL signal on each excitation/emission pair.

Therefore, one may assume that Fluorescein (BSA-FITC MBs) and Cyanine 5.5 (BSA-Cy5.5 MBs) contained samples are the most suitable for FL imaging; however, the low stability over storage time for these agents allows us to suggest samples contained Rhodamine B and Indocyanine Green (BSA-RITC MBs and BSA-ICG MBs, respectively) as the most reliable for FL imaging purposes. Furthermore, the dye chemical structure acts as a critical component of the contribution to the resulting FL signal, impacting the FL properties of agents and their concentration/stability properties.

Next, acoustic characterization reveals the possibility of using "colored" MBs as US contrast agents, as presented in Fig. 8**.** MBs with the dye-functionalized shell are tested at frequencies of 33 MHz (Fig. 8b–f) and 50 MHz (Fig. 8**h-l)**: MBs functionalized with Fluorescein (Fig. 8b, h), Rhodamine B (Fig. 8c, i), Indocyanine Green (Fig. 8d, j), Cyanine 5.5 (Fig. 8e, k) and Cyanine 7 (Fig. 8f, l) are presented under US *in vitro* imaging. Deionized water is taken as a control sample, as can be seen in Fig. 8a and g for frequencies of 50 MHz and 33 MHz, correspondingly.

All MB-containing samples revealed a significant acoustic response provided by the gaseous core of MBs. In contrast, the deionized water sample showed no acoustic response. Also, a higher concentration of produced MBs can demonstrate a higher acoustic response during US imaging, while other factors such as the narrow size distribution of produced MBs and the chemical structure of dyes may affect the proper tuning of received signals.

The optimal properties of acoustic response at the frequency of 50 MHz were observed for samples containing Rhodamine B and Indocyanine Green, as can be seen in Fig. 8c, d; and for the frequency of 33 MHz, agents contained Rhodamine B demonstrated higher acoustic response (Fig. 8i), while samples contained Fluorescein and Indocyanine Green demonstrated moderate response (Fig. 8h, j).

Thus, all samples presented in this work act as bimodal FL/US contrast agents since they are evaluated using FL tomography and US imaging. Considering the properties of MB storage stability, the efficiency of dye incorporation into the MB shell, and the size distribution properties, in our opinion, samples containing Rhodamine B (BSA-RITC MBs) and Indocyanine Green (BSA-ICG MBs) have the highest potential for further use. Both samples have optimal size distribution in the

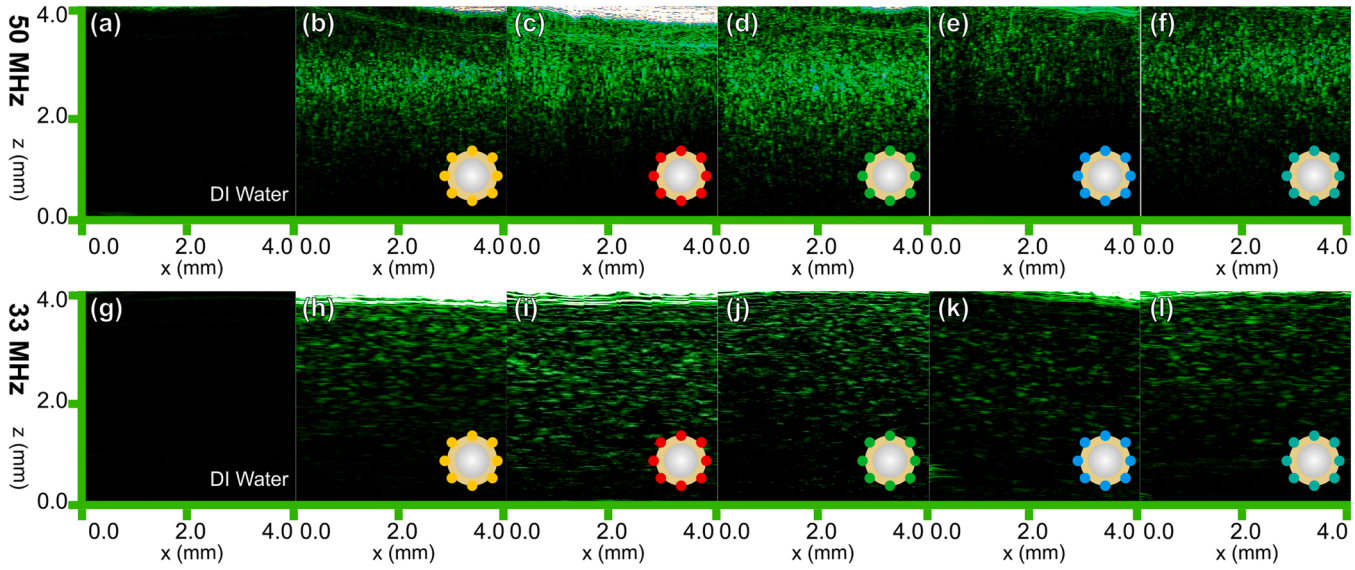

Fig. 8. US imaging at a frequency of 50 MHz for (a) DI water solution, (b) BSA-FITC MBs, (c) BSA-RITC MBs, (d) BSA-ICG MBs, (e) BSA-Cy5.5 MBs, (f) BSA-Cy7 MBs, and at a frequency of 33 MHz for (g) DI water solution, (h) BSA-FITC MBs, (i) BSA-RITC MBs, (j) BSA-ICG MBs, (k) BSA-Cy5.5 MBs, (l) BSA-Cy7 MBs, respectively.

submicron range (0.8 ± 0.4 μm), moderate concentration, prolonged stability properties (up to 47 days), and the possibility of reaching FL signal in the visible (for Rhodamine B) and NIR regions (for Indocyanine Green).

Additionally, for FL imaging applications, an urgent consideration of the effect of dye chemical structure on observed results is needed, while for US imaging, the most relevant properties of an agent are its concentration and narrow size distribution. The nature of dye chemical structure and hydrophobicity comes to the fore regarding the importance of influence on MB properties.

4. Conclusions

Dye loading into MB shell is a complex task, enjoyable from imaging (FL/US bimodal agent), physicochemical (understanding of MB interface phenomena), and pharmaceutical (model drug loading into drug-delivery systems) perspectives. A set of dye parameters (*i.e.,* chemical structure, molecular weight, and hydrophobicity) affected the properties of the albumin-dye complex (type of chemical bond between albumin and fluorophore, protein: dye ratio, solution surface tension) and other physicochemical properties of "colored" MBs (concentration, mean size, storage stability). A set of dyes is considered due to their known excellent *in vitro, in vivo*, or biomedical imaging applications (Table 1), and dyes crosslinking with protein is carried out covalently (for Fluorescein, Rhodamine, Cyanine 5.5, Cyanine 7) and electrostatically (for Indocyanine Green), for further MB production standardization. It is shown that the introduced dye hydrophobicity is inversely proportional to the value of the surface tension of the solution containing each albumin-dye complex (Fig. 1).

Protein tertiary structure change and denser packing of molecules during the US-assisted formation of MBs are confirmed by calculations and cryoTEM images (Fig. 2e). ~10^7 total protein molecules are needed to form 1 MB, and increasing dye hydrophobicity (log P) increases the number of molecules needed for MB shell formation. Fig. 3 demonstrates that MB structure enters an approximately equal ratio between the protein molecule and the albumin-dye complex despite the initial predominance of pure protein molecules in the solutions used for samples preparation.

Dye chemical structure significantly impacted "colored" MB concentration and further stability. Therefore, MBs modified with Rhodamine B and Indocyanine Green are considered optimal since they demonstrate their stability properties up to 47 days (Table S3), significant concentration over time (Fig. S4), and narrow size distribution. Furthermore, we observed that the ratio of protein: dye as 1:1 (as for Rhodamine B or Indocyanine Green in the presented work) is more favorable than higher amounts of dye to prevent fluorescence quenching on "colored" MBs, as observed for samples with a high protein-dye ratio (as BSA-Cy5.5, with the ratio of 1:5) during flow cytometry measurements presented in Fig. 6.

During FL imaging (Figs. 7, S11), we observed the impact of the fluorophores' chemical structure in the contribution to the resulting FL signal of MBs. Also, a higher concentration of produced MBs (depended on dye chemical structure) allows reaching a higher acoustic response during US imaging (Fig. 8). The protein: dye ratio of 1:1 should be accomplished for the albumin-dye complex to reach optimal physicochemical and imaging properties, as we observed for Rhodamine B and Indocyanine Green.

Thus, the presented manuscript sheds light on the proper choice of the dye for MBs production with albumin-dye complex, since dye chemical structure and hydrophobicity affect formation of albumin-dye complexes, and resulting MB properties. However, depending on each dyes required chemical and spectral properties (listed in Table 1), it is possible to use any mentioned "colored" MBs for desired (bio)imaging applications. Additionally, the presented results are helpful for further exploration of (model) drug loading into albumin-shelled MBs both in characterization and imaging perspectives, actualizing short-term clinical translation of albumin MBs as multimodal imaging or drug delivery agents.

CRediT authorship contribution statement

Roman A. Barmin: Conceptualization, Methodology, Investigation, Data curation, Visualization Writing – original draft. **Polina G. Rudakovskaya:** Methodology, Investigation, Resources, Visualization Writing – original draft. **Vasiliy S. Chernyshev:** Methodology, Investigation (Surface tension measurements), Writing – review & editing. **Olga I. Guslyakova:** Investigation (FL tomography, CLSM), Visualization. **Olga A. Sindeeva:** Investigation (FL tomography, CLSM, SEM), Visualization. **Ekaterina S. Prikhozhdenko:** Investigation (AFM), Visualization. **Daniil N. Bratashov:** Investigation (AFM), Writing – review & editing. **Arkady S. Abdurashitov:** Investigation (SEM), Visualization. **Elizaveta A. Maksimova:** Investigation (OM concentration

measurements). **Polina A. Demina:** Investigation (CryoTEM). **Evgeny V. Khaydukov:** Investigation (CryoTEM), Writing – review & editing. **Alexey V. Gayer:** Investigation (FLIM), Visualization. **Evgeny A. Shirshin:** Investigation (FLIM), Writing – review & editing. **Alexander A. Solovev:** Writing – review & editing, Funding acquisition. **Yongfeng Mei:** Writing – review & editing, Project administration, Funding acquisition. **Dmitry A. Gorin:** Writing – review & editing, Supervision, Project administration, Funding acquisition.

Declaration of Competing Interest

The authors declare that they have no known competing financial interests or personal relationships that could have appeared to influence the work reported in this paper.

Acknowledgements

This work was supported by the Russian Foundation for Basic Research (RFBR grant 19-53-80047 BRICS_t). Dynamic light scattering, zeta-potential, and fluorescent tomography measurements were performed using the equipment of the "Bioimaging and Spectroscopy" Core Facility of the Skolkovo Institute of Science and Technology. Mass-spectrometry measurements were performed using the equipment of the "Advanced Mass Spectrometry" Core Facility of the Skolkovo Institute of Science and Technology. The authors thank Dr. Ekaterina N. Obukhova and Prof. Victor G. Zgoda for their expertize and support in mass-spectrometry measurements. This work was supported by the Ministry of Science and Higher Education within the State assignment FSRC "Crystallography and Photonics" RAS in part of cryoTEM. The work on fluorescence imaging was supported by the Russian Foundation for Basic Research (grant №19-02-00947). The work of ES and AG was performed according to the Development program of the Interdisciplinary Scientific and Educational School of Lomonosov Moscow State University "Photonic and Quantum technologies. Digital medicine". The authors also would like to thank Pavel A. Belcov (Anta-Med Premium, LLC) and Dr. Kirill S. Petrov (Hadassah Medical Moscow) for their expertize and support in experiments with US imaging. The authors thank the financial support from the National Natural Science Foundation of China grants (51961145108 and 51475093).

Appendix A. Supporting information

Supplementary data associated with this article can be found in the online version at doi:10.1016/j.colsurfa.2022.129095.

References

[1] J. Mujtaba, J. Liu, K.K. Dey, T. Li, R. Chakraborty, K. Xu, D. Makarov, R.A. Barmin, D.A. Gorin, V.P. Tolstoy, G. Huang, A.A. Solovev, Y. Mei, Micro-bio-chemo-mechanical-systems: micromotors, microfluidics, and nanozymes for biomedical applications, Adv. Mater. 2007465 (2021) 1–40, https://doi.org/10.1002/adma.202007465.

[2] A.S. Timin, M.M. Litvak, D.A. Gorin, E.N. Atochina-Vasserman, D.N. Atochin, G. B. Sukhorukov, Cell-based drug delivery and use of nano-and microcarriers for cell functionalization, Adv. Healthc. Mater. 7 (2018) 1–19, https://doi.org/10.1002/adhm.201700818.

[3] M.V. Novoselova, D.V. Voronin, T.O. Abakumova, P.A. Demina, A.V. Petrov, V. V. Petrov, T.S. Zatsepin, G.B. Sukhorukov, D.A. Gorin, Focused ultrasound-mediated fluorescence of composite microcapsules loaded with magnetite nanoparticles: in vitro and in vivo study, Colloids Surf. B Biointerfaces 181 (2019) 680–687, https://doi.org/10.1016/j.colsurfb.2019.06.025.

[4] D. Nozdriukhin, N. Besedina, V. Chernyshev, O. Efimova, P. Rudakovskaya, M. Novoselova, D. Bratashov, R. Chuprov-Netochin, R. Kamyshinsky, A. Vasiliev, D. Chermoshentsev, S.A. Dyakov, V. Zharov, N. Gippius, D.A. Gorin, A. Yashchenok, Gold nanoparticle-carbon nanotube multilayers on silica microspheres: optoacoustic-Raman enhancement and potential biomedical applications, Mater. Sci. Eng. C 120 (2021), 111736, https://doi.org/10.1016/j.msec.2020.111736.

[5] R.A. Barmin, P.G. Rudakovskaya, O.I. Gusliakova, O.A. Sindeeva, E. S. Prikhozhdenko, E.A. Maksimova, E.N. Obukhova, V.S. Chernyshev, B. N. Khlebtsov, A.A. Solovev, G.B. Sukhorukov, D.A. Gorin, Air-filled bubbles stabilized by gold nanoparticle/photodynamic dye hybrid structures for theranostics, Nanomaterials 11 (2021) 1–17, https://doi.org/10.3390/nano11020415.

[6] M.V. Novoselova, D.N. Bratashov, M. Sarimollaoglu, D.A. Nedosekin, W. Harrington, A. Watts, M. Han, B.N. Khlebtsov, E.I. Galanzha, D.A. Gorin, V. P. Zharov, Photoacoustic and fluorescent effects in multilayer plasmon-dye interfaces, J. Biophotonics 12 (2019) 1–13, https://doi.org/10.1002/jbio.201800265.

[7] M.V. Novoselova, S.V. German, T.O. Abakumova, S.V. Perevoschikov, O. V. Sergeeva, M.V. Nesterchuk, O.I. Efimova, K.S. Petrov, V.S. Chernyshev, T. S. Zatsepin, D.A. Gorin, Multifunctional nanostructured drug delivery carriers for cancer therapy: Multimodal imaging and ultrasound-induced drug release, Colloids Surf. B Biointerfaces 200 (2021), 111576, https://doi.org/10.1016/j.colsurfb.2021.111576.

[8] P.N.T. Wells, Ultrasound imaging, Phys. Med. Biol. 51 (2006), https://doi.org/10.1088/0031-9155/51/13/R06.

[9] E. Stride, T. Segers, G. Lajoinie, S. Cherkaoui, T. Bettinger, M. Versluis, M. Borden, Microbubble agents: new directions, Ultrasound Med. Biol. 46 (2020) 1326–1343, https://doi.org/10.1016/j.ultrasmedbio.2020.01.027.

[10] T. Van Rooij, V. Daeichin, I. Skachkov, N. De Jong, K. Kooiman, Targeted ultrasound contrast agents for ultrasound molecular imaging and therapy, Int. J. Hyperth. 31 (2015) 90–106, https://doi.org/10.3109/02656736.2014.997809.

[11] M.A. Borden, M.L. Longo, Dissolution behavior of lipid monolayer-coated, air-filled microbubbles: effect of lipid hydrophobic chain length, Langmuir 18 (2002) 9225–9233, https://doi.org/10.1021/la026082h.

[12] P.V. Chitnis, S. Koppolu, L. Mamou, C. Chlon, J.A. Ketterling, Influence of shell properties on high- frequency ultrasound imaging and drug, IEEE Trans. Ultrason. Ferroelectr. Freq. Control. 60 (2013) 53–64.

[13] S. Himuro, Physicochemical characteristics of microbubbles, Kagaku Koguku 71 (2007) 165–169, https://doi.org/10.1179/175889709X446507.Microbubble.

[14] D. Grishenkov, L. Kari, L.Å. Brodin, T.B. Brismar, G. Paradossi, In vitro contrast-enhanced ultrasound measurements of capillary microcirculation: comparison between polymer- and phospholipid-shelled microbubbles, Ultrasonics 51 (2011) 40–48, https://doi.org/10.1016/j.ultras.2010.05.006.

[15] T. Segers, N. de Jong, M. Versluis, Uniform scattering and attenuation of acoustically sorted ultrasound contrast agents: modeling and experiments, J. Acoust. Soc. Am. 140 (2016) 2506–2517, https://doi.org/10.1121/1.4964270.

[16] S. Qin, C.F. Caskey, K.W. Ferrara, Ultrasound contrast microbubbles in imaging and therapy: physical principles and engineering, Phys. Med. Biol. 54 (2009), https://doi.org/10.1088/0031-9155/54/6/R01.

[17] L. Hoff, Acoustic properties of ultrasonic contrast agents, Ultrasonics 34 (1996) 591–593, https://doi.org/10.1016/0041-624X(96)00035-2.

[18] S. Sridhar, A. Patel, S.V. Dalvi, Estimation of storage stability of aqueous microbubble suspensions, Colloids Surf. A Physicochem. Eng. Asp. 489 (2016) 182–190, https://doi.org/10.1016/j.colsurfa.2015.10.044.

[19] W.K. Chong, V. Papadopoulou, P.A. Dayton, Imaging with ultrasound contrast agents: current status and future, Abdom. Radiol. 43 (2018) 762–772, https://doi.org/10.1007/s00261-018-1516-1.

[20] G. Köse, M. Darguzyte, F. Kiessling, Molecular ultrasound imaging, Nanomaterials 10 (2020) 1–28, https://doi.org/10.3390/nano10101935.

[21] A. Upadhyay, S.V. Dalvi, Microbubble formulations: synthesis, stability, modeling and biomedical applications, Ultrasound Med. Biol. 45 (2019) 301–343, https://doi.org/10.1016/j.ultrasmedbio.2018.09.022.

[22] Y. Li, Y. Chen, M. Du, Z.Y. Chen, Ultrasound technology for molecular imaging: from contrast agents to multimodal imaging, ACS Biomater. Sci. Eng. 4 (2018) 2716–2728, https://doi.org/10.1021/acsbiomaterials.8b00421.

[23] T.B. Brismar, D. Grishenkov, B. Gustafsson, J. Härmark, Å. Barrefelt, S.V.V. N. Kothapalli, S. Margheritelli, L. Oddo, K. Caidahl, H. Hebert, G. Paradossi, Magnetite nanoparticles can be coupled to microbubbles to support multimodal imaging, Biomacromolecules 13 (2012) 1390–1399, https://doi.org/10.1021/bm300099f.

[24] Å. Barrefelt, Y. Zhao, M.K. Larsson, G. Egri, R.V. Kuiper, J. Hamm, M. Saghafian, K. Caidahl, T.B. Brismar, P. Aspelin, R. Heuchel, M. Muhammed, L. Dähne, M. Hassan, Fluorescence labeled microbubbles for multimodal imaging, Biochem. Biophys. Res. Commun. 464 (2015) 737–742, https://doi.org/10.1016/j.bbrc.2015.07.017.

[25] A.A. Doinikov, A. Bouakaz, Review of shell models for contrast agent microbubbles, IEEE Trans. Ultrason. Ferroelectr. Freq. Control. 58 (2011) 981–993, https://doi.org/10.1109/TUFFC.2011.1899.

[26] K. Murayama, M. Tomida, Heat-induced secondary structure and conformation change of bovine serum albumin investigated by Fourier transform infrared spectroscopy, Biochemistry 43 (2004) 11526–11532, https://doi.org/10.1021/bi0489154.

[27] A. Upadhyay, S.V. Dalvi, Synthesis, characterization and stability of BSA-encapsulated microbubbles, RSC Adv. 6 (2016) 15016–15026, https://doi.org/10.1039/c5ra24304a.

[28] M.J. Borrelli, W.D. O'Brien, L.J. Bernock, H.R. Williams, E. Hamilton, J. Wu, M. L. Oelze, W.C. Culp, Production of uniformly sized serum albumin and dextrose microbubbles, Ultrason. Sonochem. 19 (2012) 198–208, https://doi.org/10.1016/j.ultsonch.2011.05.010.

[29] M.W. Keller, W. Glasheen, S. Kaul, Albunex: a safe and effective commercially produced agent for myocardial contrast echocardiography, J. Am. Soc. Echocardiogr. 2 (1989) 48–52, https://doi.org/10.1016/S0894-7317(89)80028-8.

[30] T.A.M. Rovers, G. Sala, E. van der Linden, M.B.J. Meinders, Temperature is key to yield and stability of BSA stabilized microbubbles, Food Hydrocoll. 52 (2016) 106–115, https://doi.org/10.1016/j.foodhyd.2015.05.038.

[31] S.V. Dalvi, A.H. Khan, X. Jiang, S. Surwase, M. Gultekinoglu, C. Bayram, I. Sathisaran, D. Bhatia, J. Ahmed, B. Wu, K. Ulubayram, M. Edirisinghe, Effectiveness of Oil-layered Albumin Microbubbles Produced Using Microfluidic t-Junctions in Series for In Vitro Inhibition of Tumor Cells, 2020. ⟨https://doi.org/10.1021/acs.langmuir.0c01557⟩.
[32] A.H. Khan, S.V. Dalvi, Kinetics of Albumin Microbubble Dissolution in Aqueous Media, 2020. ⟨https://doi.org/10.1039/c9sm01516g⟩.
[33] Q. Wang, C. Xue, H. zhao, Y. Qin, X. Zhang, Y. Li, The fabrication of protein microbubbles with diverse gas core and the novel exploration on the role of interface introduction in protein crystallization, Colloids Surf. A Physicochem. Eng. Asp. 589 (2020), 124471, https://doi.org/10.1016/j.colsurfa.2020.124471.
[34] M.K. Alhasan, L. Liu, M.A. Lewis, J. Magnusson, R.P. Mason, Comparison of optical and power doppler ultrasound imaging for non-invasive evaluation of arsenic trioxide as a vascular disrupting agent in tumors, PLoS One 7 (2012), https://doi.org/10.1371/journal.pone.0046106.
[35] A.V. DSouza, H. Lin, E.R. Henderson, K.S. Samkoe, B.W. Pogue, Review of fluorescence guided surgery systems: identification of key performance capabilities beyond indocyanine green imaging, J. Biomed. Opt. 21 (2016), 080901, https://doi.org/10.1117/1.jbo.21.8.080901.
[36] R.X. Xu, J. Huang, J.S. Xu, D. Sun, G.H. Hinkle, E.W. Martin, S.P. Povoski, Fabrication of indocyanine green encapsulated biodegradable microbubbles for structural and functional imaging of cancer, J. Biomed. Opt. 14 (2009), 034020, https://doi.org/10.1117/1.3147424.
[37] Y. Li, W. Huang, C. Li, X. Huang, Indocyanine green conjugated lipid microbubbles as an ultrasound-responsive drug delivery system for dual-imaging guided tumor-targeted therapy, RSC Adv. 8 (2018) 33198–33207, https://doi.org/10.1039/C8RA03193B.
[38] L.D. Lavis, Teaching old dyes new tricks: biological probes built from fluoresceins and rhodamines, Annu. Rev. Biochem. 86 (2017) 825–843, https://doi.org/10.1146/annurev-biochem-061516-044839.
[39] Q. Yang, Z. Ma, H. Wang, B. Zhou, S. Zhu, Y. Zhong, J. Wang, H. Wan, A. Antaris, R. Ma, X. Zhang, J. Yang, X. Zhang, H. Sun, W. Liu, Y. Liang, H. Dai, Rational design of molecular fluorophores for biological imaging in the NIR-II window, Adv. Mater. 29 (2017), https://doi.org/10.1002/adma.201605497.
[40] S. Luo, E. Zhang, Y. Su, T. Cheng, C. Shi, A review of NIR dyes in cancer targeting and imaging, Biomaterials 32 (2011) 7127–7138, https://doi.org/10.1016/j.biomaterials.2011.06.024.
[41] J.T. Alander, I. Kaartinen, A. Laakso, T. Pätilä, T. Spillmann, V.V. Tuchin, M. Venermo, P. Välisuo, A review of indocyanine green fluorescent imaging in surgery, Int. J. Biomed. Imaging (2012)) (2012), https://doi.org/10.1155/2012/940585.
[42] M.B. Reinhart, C.R. Huntington, L.J. Blair, B.T. Heniford, V.A. Augenstein, Indocyanine green:historical context, current applications, and future considerations, Surg. Innov. 23 (2016) 166–175, https://doi.org/10.1177/1553350615604053.
[43] E.A. te Velde, T. Veerman, V. Subramaniam, T. Ruers, The use of fluorescent dyes and probes in surgical oncology, Eur. J. Surg. Oncol. 36 (2010) 6–15, https://doi.org/10.1016/j.ejso.2009.10.014.
[44] J.R. Lindner, P.A. Dayton, M.P. Coggins, K. Ley, J. Song, K. Ferrara, S. Kaul, Noninvasive imaging of inflammation by ultrasound detection of Phagocytosed microbubbles, Circulation 102 (2000) 531–538, https://doi.org/10.1161/01.CIR.102.5.531.
[45] E.J. Park, Y.Z. Zhang, N. Vykhodtseva, N. McDannold, Ultrasound-mediated blood-brain/blood-tumor barrier disruption improves outcomes with trastuzumab in a breast cancer brain metastasis model, J. Control. Release 163 (2012) 277–284, https://doi.org/10.1016/j.jconrel.2012.09.007.
[46] L. Wang, Y. Hu, Q. Peng, J. Zhou, Q. Zhou, S. An, C. Niu, Indocyanine-green-loaded microbubbles for localization of sentinel lymph node using near-infrared fluorescence/ultrasound imaging: a feasibility study, RSC Adv. 6 (2016) 50513–50520, https://doi.org/10.1039/c5ra26814a.
[47] L. Mai, A. Yao, J. Li, Q. Wei, M. Yuchi, X. He, M. Ding, Q. Zhou, Cyanine 5.5 conjugated nanobubbles as a tumor selective contrast agent for dual ultrasound-fluorescence imaging in a Mouse Model, PLoS One 8 (2013) 1–10, https://doi.org/10.1371/journal.pone.0061224.
[48] M. Liu, A. Dasgupta, P. Koczera, S. Schipper, D. Rommel, Y. Shi, F. Kiessling, T. Lammers, Drug loading in poly(butyl cyanoacrylate)-based polymeric microbubbles, Mol. Pharm. 17 (2020) 2840–2848, https://doi.org/10.1021/acs.molpharmaceut.0c00242.
[49] R.A. Barmin, P.G. Rudakovskaya, V.S. Chernyshev, O.I. Guslyakova, P.A. Belcov, E. N. Obukhova, A.V. Gayer, E.A. Shirshin, D.A. Gorin, Optoacoustic/fluorescent/acoustic imaging probe based on air-filled bubbles functionalized with gold nanorods and fluorescein isothiocyanate, ACS Omega 6 (2021) 3809–3821, https://doi.org/10.1021/acsomega.0c05518.
[50] V.F. Korolovych, O.A. Grishina, O.A. Inozemtseva, A.V. Selifonov, D.N. Bratashov, S.G. Suchkov, L.A. Bulavin, O.E. Glukhova, G.B. Sukhorukov, D.A. Gorin, Impact of high-frequency ultrasound on nanocomposite microcapsules: In silico and in situ visualization, Phys. Chem. Chem. Phys. 18 (2015) 2389–2397, https://doi.org/10.1039/c5cp05465f.
[51] PubChem, Fluorescein (Compound Summary), (n.d.). ⟨https://pubchem.ncbi.nlm.nih.gov/compound/Fluorescein⟩.
[52] PubChem, Rhodamine B (Compound Summary), (n.d.). ⟨https://pubchem.ncbi.nlm.nih.gov/compound/6694⟩.
[53] PubChem, Indocyanine Green (Compound Summary), (n.d.). ⟨https://pubchem.ncbi.nlm.nih.gov/compound/6096882⟩.
[54] I.V. Tetko, V.Y. Tanchuk, Application of associative neural networks for prediction of lipophilicity in ALOGPS 2.1 program, J. Chem. Inf. Comput. Sci. 42 (2002) 1136–1145, https://doi.org/10.1021/ci025515j.
[55] R. Sjöback, J. Nygren, M. Kubista, Absorption and fluorescence properties of fluorescein, Spectrochim. Acta Part A Mol. Spectrosc. 51 (1995), https://doi.org/10.1016/0584-8539(95)01421-P.
[56] R.F. Kubin, A.N. Fletcher, Fluorescence quantum yields of some rhodamine dyes, J. Lumin. 27 (1982) 455–462, https://doi.org/10.1016/0022-2313(82)90045-X.
[57] R. Philip, A. Penzkofer, W. Bäumler, R.M. Szeimies, C. Abels, Absorption and fluorescence spectroscopic investigation of indocyanine green, J. Photochem. Photobiol. A Chem. 96 (1996) 137–148, https://doi.org/10.1016/1010-6030(95)04292-X.
[58] Lumiprobe, Cy5.5-NHS-ester Product Information, (n.d.). ⟨https://www.lumiprobe.com/p/cy55-nhs-ester⟩.
[59] Lumiprobe, Cy7-NHS-ester (Product Information), (n.d.). ⟨https://www.lumiprobe.com/p/cy7-nhs-ester⟩.
[60] T.A.M. Rovers, G. Sala, E. Van Der Linden, M.B.J. Meinders, Effect of Temperature and pressure on the stability of protein microbubbles, ACS Appl. Mater. Interfaces 8 (2016) 333–340, https://doi.org/10.1021/acsami.5b08527.
[61] T.A.M. Rovers, G. Sala, E. Van der Linden, M.B.J. Meinders, Potential of microbubbles as fat replacer: effect on rheological, tribological and sensorial properties of model food systems, J. Texture Stud. 47 (2016) 220–230, https://doi.org/10.1111/jtxs.12175.
[62] E.A. Maksimova, R.A. Barmin, P.G. Rudakovskaya, O.A. Sindeeva, E. S. Prikhozhdenko, A.M. Yashchenok, B.N. Khlebtsov, A.A. Solovev, G. Huang, Y. Mei, K.K. Dey, D.A. Gorin, Air-filled microbubbles based on albumin functionalized with gold nanocages and zinc phthalocyanine for multimodal imaging, Micromachines 12 (2021) 1161, https://doi.org/10.3390/mi12101161..
[63] A.K. Wright, M.R. Thompson, Hydrodynamic structure of bovine serum albumin determined by transient electric birefringence, Biophys. J. 15 (1975) 137–141, https://doi.org/10.1016/S0006-3495(75)85797-3.
[64] M.W. Grinstaff, K.S. Suslick, Air-filled proteinaceous microbubbles: synthesis of an echo-contrast agent, Proc. Natl. Acad. Sci. USA, 88 (1991) 7708–7710. ⟨https://doi.org/10.1073/pnas.88.17.7708⟩.
[65] F. Cavalieri, M. Ashokkumar, F. Grieser, F. Caruso, Ultrasonic synthesis of stable, functional lysozyme microbubbles, Langmuir 24 (2008) 10078–10083, https://doi.org/10.1021/la801093q.
[66] Sigalit Avivi, Aharon Gedanken Proteinaceous, Microspheres: the case of streptavidin, Biochem. J. 366 (2002) 705–707, https://doi.org/10.1042/bj20020676.
[67] L. Zhu, F. Yang, L. Chen, E.J. Meehan, M. Huang, A new drug binding subsite on human serum albumin and drug-drug interaction studied by X-ray crystallography, J. Struct. Biol. 162 (2008) 40–49, https://doi.org/10.1016/j.jsb.2007.12.004.
[68] L.R.S. Barbosa, M.G. Ortore, F. Spinozzi, P. Mariani, S. Bernstorff, R. Itri, The importance of protein-protein interactions on the pH-induced conformational changes of bovine serum albumin: a small-angle x-ray scattering study, Biophys. J. 98 (2010) 147–157, https://doi.org/10.1016/j.bpj.2009.09.056.
[69] S.F. Santos, D. Zanette, H. Fischer, R. Itri, A systematic study of bovine serum albumin (BSA) and sodium dodecyl sulfate (SDS) interactions by surface tension and small angle X-ray scattering, J. Colloid Interface Sci. 262 (2003) 400–408, https://doi.org/10.1016/S0021-9797(03)00109-7.
[70] J. Park, D. Park, U. Shin, S. Moon, C. Kim, H.S. Kim, H. Park, K. Choi, B.K. Jung, J. Oh, J. Seo, Synthesis of laboratory ultrasound contrast agents, Molecules 18 (2013) 13078–13095, https://doi.org/10.3390/molecules181013078.
[71] S. Diego, Higher harmonics of vibrating gas-filled microspheres. Part two : measurements transducer Albunex plate, Ultrasonics 32 (1994) 455–459, https://doi.org/10.1016/0041-624X(94)90065-5.
[72] A.A. Doinikov, P.A. Dayton, Spatio-temporal dynamics of an encapsulated gas bubble in an ultrasound field, J. Acoust. Soc. Am. 120 (2006) 661–669, https://doi.org/10.1121/1.2215228.
[73] H.B. Levene, R. Moision, E. Villapando, J. Torgerson, J. Maniquis, R. Kleinhenz, R. Keen, J.L. Barnhart, Characterization of Albunex®, J. Acoust. Soc. Am. 87 (1990) S69–S70, https://doi.org/10.1121/1.2028331.
[74] J. Barnhart, H. Levene, E. Villapando, J. Maniquis, J. Fernandez, S. Rice, E. Jablonski, T. Gjøen, H. Tolleshaug, Characteristics of Albunex air-filled albumin microspheres for echocardiography contrast enhancement, Investig. Radiol. 25 (1990) S162–S164, https://doi.org/10.1097/00004424-199009001-00070.
[75] M. Zhou, F. Cavalieri, M. Ashokkumar, Tailoring the properties of ultrasonically synthesised microbubbles, Soft Matter 7 (2011) 623–630, https://doi.org/10.1039/c0sm00652a.
[76] W. He, F. Yang, Y. Wu, S. Wen, P. Chen, Y. Zhang, N. Gu, Microbubbles with surface coated by superparamagnetic iron oxide nanoparticles, Mater. Lett. 68 (2012) 64–67, https://doi.org/10.1016/j.matlet.2011.10.013.
[77] I. Kucuk, N.F. Yilmaz, A. Sinan, Effects of junction angle and gas pressure on polymer nanosphere preparation from microbubbles bursted in a combined microfluidic device with thin capillaries, J. Mol. Struct. 1173 (2018) 422–427, https://doi.org/10.1016/j.molstruc.2018.06.084.
[78] X. Zhao, X. Zhang, L. Xue, J. Wang, B. Shen, C. Luo, Q. Wang, Preparation and in vivo evaluation of ligand-conjugated polymeric microbubbles as targeted ultrasound contrast agents, Colloids Surf. A Physicochem. Eng. Asp. 452 (2014) 59–64, https://doi.org/10.1016/j.colsurfa.2014.03.082.
[79] N.A. Hosny, G. Mohamedi, P. Rademeyer, J. Owen, Y. Wu, M.X. Tang, R.J. Eckersley, E. Stride, M.K. Kuimova, Mapping microbubble viscosity using

fluorescence lifetime imaging of molecular rotors, Proc. Natl. Acad. Sci. USA, 110 (2013) 9225–9230. ⟨https://doi.org/10.1073/pnas.1301479110⟩.

[80] Y. Liu, J.A. Feshitan, M.-Y. Wei, M.A. Borden, B. Yuan, Ultrasound-modulated fluorescence based on fluorescent microbubbles, J. Biomed. Opt. 19 (2014), 085005, https://doi.org/10.1117/1.jbo.19.8.085005.

[81] M.D. Mokrousov, M.V. Novoselova, J. Nolan, W. Harrington, P. Rudakovskaya, D. N. Bratashov, E.I. Galanzha, J.P. Fuenzalida-Werner, B.P. Yakimov, G. Nazarikov, V.P. Drachev, E.A. Shirshin, V. Ntziachristos, A.C. Stiel, V.P. Zharov, D.A. Gorin, Amplification of photoacoustic effect in bimodal polymer particles by self-quenching of indocyanine green, Biomed. Opt. Express 10 (2019) 4775, https://doi.org/10.1364/boe.10.004775.